Revue des Composites et des Matériaux Avancés-Journal of Composite and Advanced Materials
Vol. 36, No. 5, October, 2026, pp. 1103-1109
Journal homepage: http://iieta.org/journals/rcma

Influence of Pulsed-TIG Welding Frequency on the Quality of 304L Joint

Basim Al-Bhadle[1], Affaan Uthman Moosa[1], Suad H. Abbas Raubye[2*]

[1] Engineering Technical College-Baghdad, Middle Technical University, Baghdad 10001, Iraq
[2] Electromechanical Engineering College, University of Technology, Baghdad 10066, Iraq

Corresponding Author Email: suad.h.abbas@uotechnology.edu.iq

Copyright: ©2026 The authors. This article is published by IIETA and is licensed under the CC BY 4.0 license (http://creativecommons.org/licenses/by/4.0/).

https://doi.org/10.18280/rcma.360516

Received: 1 June 2026
Revised: 19 July 2026
Accepted: 31 July 2026
Available online: 31 October 2026

Keywords:
tungsten inert gas welding, 304L, pulse, heat-affected zone

ABSTRACT

Tungsten inert gas (TIG) welding is widely used due to its superior precision and ability to produce high-quality, defect-free joints. This research investigates the impact of current mode on mechanical properties, microstructure, and corrosion resistance in similar 304L joints. A comparison between continuous direct current (CDC) and pulsed direct current (PDC) was conducted at various frequencies (100, 200, and 300 Hz) with 60 A peak current, 12 L/min Argon shielding gas, ER308L filler rod, and a thoriated tungsten electrode (EWTH-1). Tensile testing and microhardness testing evaluated the mechanical properties. An optical microscope was used to examine the microstructure. The ultimate tensile strength (UTS) for CDC and PDC at 100 Hz was decreased by about 33.5% compared to the base metal (BM) (735 MPa). For high frequencies of 200 and 300 Hz retained about 93% of the BM strength and increased a ductility paradox. The failure strain these high frequency samples reached for 0.58. This value significantly surpasses both the BM (0.49) and the CDC weld (0.31). The results demonstrate simultaneous improvement in both strength and ductility at high pulsing frequencies conditions. A more uniform hardness distribution across the weldment was achieved in the 300 Hz PDC, contrasting with the softened weld zone (WZ) (191.5 HV) and highly irregular heat-affected zone (HAZ) peaks (up to 223 HV) found in CDC welds. Microstructural analysis confirmed that high-frequency pulsing refined the solidification morphology, transitioning from coarse columnar dendrites to a dense, fine dendritic network. In contrast, the CDC and 100 Hz PDC samples showed significant grain coarsening in both the WZ and HAZ, which directly correlates with their premature tensile failure. Corrosion results indicated that the refined microstructure in the WZ and narrowed HAZ for 300PDC increased corrosion resistance by 67% compared to the CDC joint. It is hypothesized that this improvement is attributed to a favorable delta ferrite phase balance and the maintaining the protective passive film enriched with chromium. Further chemical analysis is required to confirm these mechanisms.

1. INTRODUCTION

304L is one of the austenitic stainless steel used widely throughout major industries [1-3]. It is used in automotive production and thermal power. It is also applied in aerospace and pressure vessel construction [1, 4, 5]. 304L is largely adopted due to its resistance to intergranular corrosion and superior fracture toughness under harsh acidic conditions [2, 3, 6].

The performance of 304 depends on the integrity of welded joints [1, 2]. Conventional welding methods often generate a wide heat-affected zone (HAZ). The width of this zone reduces overall joint strength [1, 5]. Thermal degradation degrades weld quality by reducing resistance to crack propagation. This elevated risk of cracking shortens the service life of pressure equipment [1, 4]. The Selection of welding process is essential to maintain the balance of alloying elements in 304L stainless steel. The sound weld joint is reflected in the microstructure and the serviceable performance [1-3]. Tungsten inert gas (TIG) welding is used to join thin to medium gauge sections [4, 7, 8]. Fine control over heat input during TIG process enhances the mechanical strength of joints [4, 8]. This welding process is used to perform the root pass in pipeline. Full joint soundness remains essential in piping structures [8, 9].

Low process efficiency and limited electrode thermal capacity are major limitations of TIG welding for thin plates. High welding currents cause excessive arc pressure and thermal distortion [4, 6, 8]. Pulsed current tungsten inert gas (PCTIG) welding alternates between peak and base currents. The pulse technique decreases the thermal damage and increases weld penetration [1, 6, 10-12]. The pulse frequency is an effective parameter in pulsed current welding. Appropriate frequency improves the joint microstructure and arc welding pressure [7, 10, 11]. Previous research modeled pulse current gas tungsten arc welding (PCGTAW) using

dynamic finite element heat source model. The study results pointed that Pulse frequency directly controls transient temperature distributions during processing [13]. Applying a 5 kHz pulsed current improved TIG welding joint by reducing weld porosity and refining the microstructure of the weld zone (WZ) [14]. The use of pulsed current modifies the WZ microstructure by promoting a fine equiaxed grain structure and optimizing delta ferrite (δ-ferrite) distribution [15].

Arc pulsation frequency significantly affects the solidification behavior of the melt. Increasing the pulsation frequency breaks up dendritic arm. This mechanism promotes grain refinement to produce an optimized microstructure [6, 7, 10]. More refine microstructure is important to improve the joints mechanical properties [2, 4, 10]. Other studies evaluated the effect of process parameters including welding travel speed and welding current as well as shielding gas compositions (e.g., nitrogen-argon mixtures) on bead geometry and δ-ferrite content. The variation of frequencies has a significant effect on the microstructure of 304L [6, 9, 16].

This study examines the effect of pulse frequency on the mechanical and microstructural integrity of 304L joints. It analytically evaluates the relationship between pulse frequency and grain refinement along with overall joint strength. This investigation also assesses the efficacy of pulsed TIG parameters to produce sound welds devoid of defects as required in industrial applications [6, 10, 16].

2. EXPERIMENTAL WORK

The stainless steel grade selected for this investigation was Type 304L. The dimensions of the sheets were 120 × 60 × 2 mm, and their chemical composition is listed in Table 1.

Table 1. Chemical composition of 304L

Elements	wt.%
C	0.02
Si	0.478
Mn	0.97
P	0.0126
S	0.0015
Cr	18.7
Ni	8.57
Fe	Balance

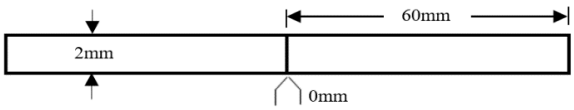


Figure 1. Design of butt welding joint

The butt joint configuration is shown in Figure 1. Based on the thickness of the material, a 1.6 mm diameter EWTH-1 thoriated tungsten electrode was selected. The TIG welding machine used in this study was a MATRIX 400 AC/DC high-frequency machine. It provides complete digital control over all welding parameters. The electrode tip was ground into a 30° cone with a 3.2 mm tapered length prior to welding. This electrode type generated a stable and concentrated arc during the welding process and effectively prevented excessive heating and electrode burning. The 12 L/min gas flow rate provided an inert environment to prevent embrittlement caused by atmospheric contamination. 308L filler metal was utilized; these slightly over-alloyed fillers ensured a ductile weld bead that accommodates higher plastic deformation than the base metal (BM).

Pulse direct current TIG welding features highly adjustable operating variables. This characteristic precise control over total heat generation during welding process. For this investigation four joints were welded using the specific parameters listed in Table 2. The welding voltage, thermal efficiency, and welding speed are 20 V, 0.6, and ~7 mm/sec, respectively. Figure 2 displays the weldment profile for each condition.

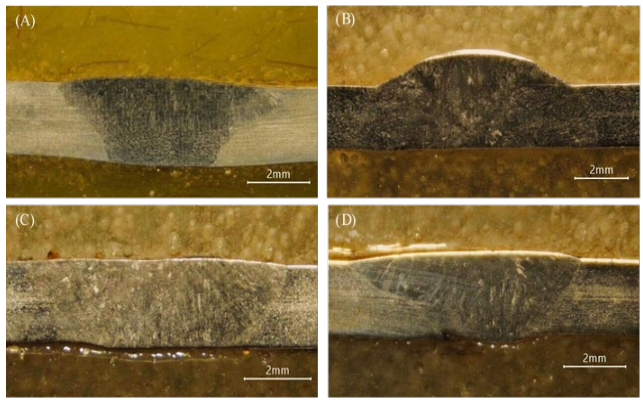


Figure 2. Weldment profile for (A) CDC, (B) 100PDC, (C) 200PDC, and (D) 300PDC
Note: Continuous direct current (CDC), pulsed direct current (PDC).

All cross-section dimensions of the joint are listed in Table 3. The cup bead width was reduced from 4.25 ± 0.15 mm to 3.45 ± 0.10 mm by increasing the pulse frequency from 0 Hz (continuous direct current (CDC)) to 300 Hz (300 pulsed direct current (PDC)). The HAZ width decreased by more than half from 1.15 ± 0.10 mm to 0.50 ± 0.06 mm as a result of the lower net heat input associated with pulsed current modes. In addition, the height of reinforcement remained consistently low across the high-frequency and CDC welds (0.15–0.20 mm) to minimize geometric stress concentration sites at the weld toes.

Following the welding process, test specimens for tensile, microhardness, cross-section metallographic, and corrosion tests were extracted using waterjet cutting to minimize thermal distortion.

Room-temperature tensile tests were performed on flat specimens designed in accordance with American Society for Testing and Materials (ASTM) E8 for the BM (Figure 3(a)) [17] and standard transverse tensile testing procedures for welded joints (Figure 3(b)) [18]. All tensile specimens featured a gauge length of 25 mm. Tensile tests carried out at a displacement rate 1 mm/min. Strain was calculated from machine crosshead displacement.

The average results of three samples were used to evaluate the ultimate tensile strength (UTS) and failure strain, while the stress-strain behavior of the welded joints was compared directly to that of the 304L BM.

Vickers microhardness testing was performed using an HVS-1000ZCM-XY tester (Suoyan, Shanghai, China). A load of 100 gf was applied for a dwell time of 15 s. Indentations were positioned at 0.5 mm intervals from the weld center to the BM mapping of hardness distribution across metallurgical zones is depicted in Figure 4.

Metallographic and corrosion specimens were mounted. They were ground and polished to a mirror condition. The polished surfaces were etched for approximately 60 s. The

reagent solution contains 20 mL HCl, 10 mL HNO_3, and 44 mL H_2O [19]. Optical microscopy (OM) was performed to characterize the microstructure.

Table 2. Welding parameters and calculated values.

Welding Parameters	Peak Current (A)	Background Current (A)	Pulse Frequency (Hz)	Duty Cycle (%)	Pulse Width (ms)	Average Current (A)	Heat Input (J/mm)
CDC	60	-	-	100	0	60	102.8
100PDC	60	0	100	60	6	36	61.7
200PDC	60	0	200	60	3	36	61.7
300PDC	60	0	300	60	2	36	61.7

Note: Continuous direct current (CDC), pulsed direct current (PDC).

Table 3. Weldment cross-sectional dimensions

Penetration Depth (mm)	Bead Width (mm)	Reinforcement Height (mm)	HAZ Width (mm)	Penetration Depth (mm)
CDC	2.01 ± 0.05	4.25 ± 0.15	0.15 ± 0.04	1.15 ± 0.10
100PDC	2.02 ± 0.06	4.60 ± 0.18	0.55 ± 0.08	1.05 ± 0.12
200PDC	2.00 ± 0.04	3.85 ± 0.12	0.20 ± 0.05	0.75 ± 0.08
300PDC	2.01 ± 0.05	3.45 ± 0.10	0.18 ± 0.05	0.50 ± 0.06

Note: Continuous direct current (CDC), pulsed direct current (PDC), heat-affected zone (HAZ).

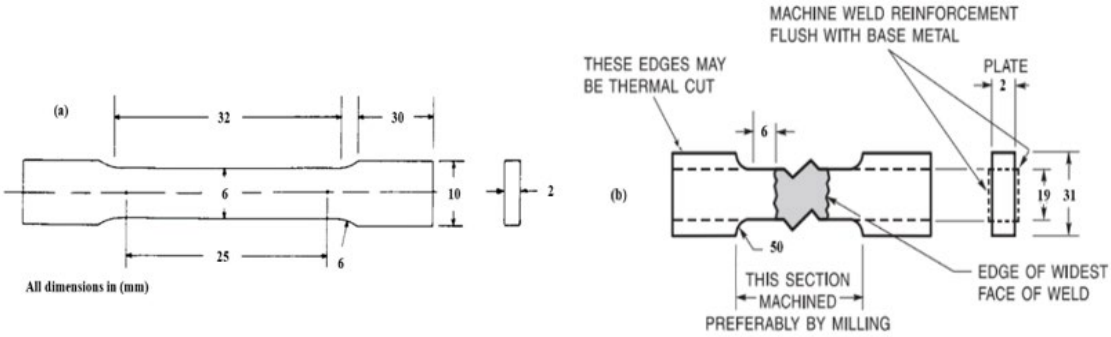


Figure 3. Tensile test specimens for (a) Base metal and (b) welded joint

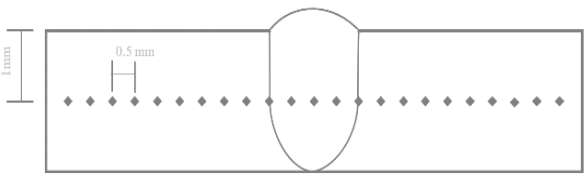


Figure 4. Hardness distribution map

Electrochemical measurements were carried out in a conventional electrochemical cell. The cell featured a fiberglass casing with a 7 mm diameter opening.

A PARSTAT 2273 potentiostat/galvanostat system was used to investigate the corrosion behavior of the weldments. Corrosion rate calculations followed the ASTM G102-89 standard [20]. The open circuit potential (OCP) measurement continued for 30 minutes. The system reached stationary equilibrium during this period. The potentiodynamic scan ranged from the initial value of -2 V to the final value of -0.1 V versus the reference electrode. The scan rate was 1 mV/s. All tests were conducted in a corrosion cell containing an aqueous solution of 3.5 wt.% NaCl.

3. DISCUSSION

The experimental results investigate the effect of the changing the welding current mode from continuous to pulsed. The pulsed conditions were operated with a zero-background current. Arc stability was visually verified during welding. The absence of real-time oscilloscope or high-speed optical monitoring represents a study limitation because zero-background settings can potentially influence arc stability at higher pulse frequencies. This section presents the mechanical and microstructural characterization results of the 2 mm 304L stainless steel joints. The findings explain the superior performance associated with increasing the pulsing frequency.

3.1 Tensile properties and energy absorption

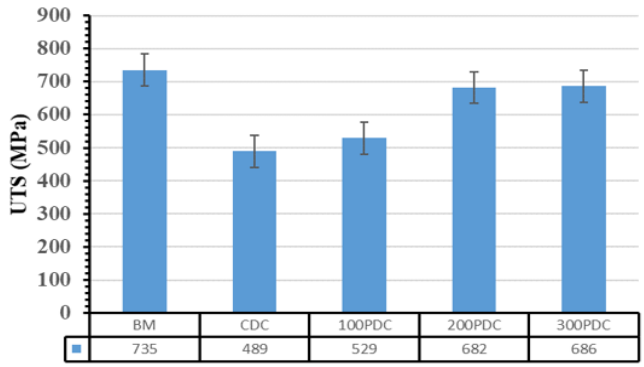


Figure 5. UTS for BM, CDC, and PDC at frequencies of 100, 200, and 300 Hz

Note: Ultimate tensile strength (UTS), base metal (BM), Continuous direct current (CDC), pulsed direct current (PDC).

Figure 5 and Figure 6 illustrate the increase in joint tensile strength with increasing the pulse frequencies. The UTS of

BM reaches 735 MPa. Minor strain hardening from previous manufacturing operations cause this increase. The residual cold work generated deformation twins within the microstructure. The twins acted as robust obstacles to dislocation mobility. This effect reduces the failure strain to 0.49. The CDC sample displayed the lowest UTS of 489 MPa. The UTS of CDC represents a reduction 33.5% from the UTS of BM. Pulsed current progressively improved joint strength. The 200PDC specimen achieved 682 MPa. The 300PDC specimen recorded a strength 686 MPa. The 200PDC and 300PDC samples restore approximately 93% of the UTS for the base metal. Both 200PDC and 300PDC current modes improve a failure strain of 0.58. This combination of optimization of tensile strength and enhanced ductility is directly supported by the refined grain morphology observed in the microstructure, which prevents premature brittle failure.

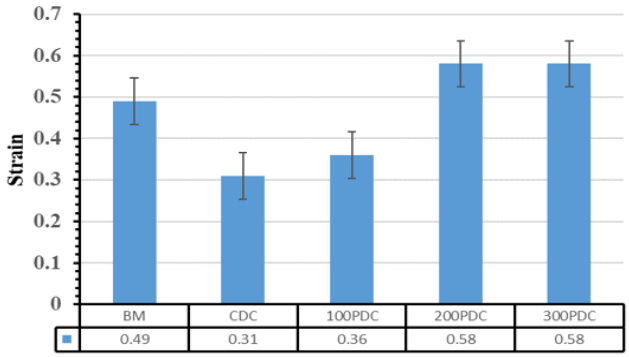


Figure 6. Strain for BM, CDC, and PDC at frequencies of 100, 200, and 300 Hz
Note: Base metal (BM), continuous direct current (CDC), pulsed direct current (PDC).

3.2 Microstructural refinement and solidification

The microstructural analysis in Figure 7 provides a physical explanation for the observed mechanical behavior. To illustrates the correlation between grain morphology and tensile performance. The BM exhibits a fine equiaxed austenitic (γ-phase) microstructure with a face centered cubic (FCC) crystal lattice. The dissolution of high concentrations of chromium and nickel within the iron matrix generates solid solution strengthening. Minor cold working generates twin bands. These twin bands act as robust microstructural barriers to dislocation motion. They significant increase in the UTS.

A coarse columnar dendritic structure is clearly visible in the CDC and 100PDC micrographs. The CDC joint has a primary dendrite spacing (λ1) of 28.4 ± 3.1 and secondary dendrite spacing (λ2) of 9.6 ± 1.2. The 100PDC joint microstructure shows a primary dendrite spacing λ1 of 24.2 ± 2.8 and secondary dendrite spacing λ2 of 8.1 ± 1. The relatively high heat input and slow cooling rate cause the grains to grow from the welding edges directly toward the weld centerline. This growth forms long aligned dendrites. Pulsed current modes at 200 Hz and 300 Hz refine the weld microstructure. The λ1 decreases to 18.6 ± 1.9 for 200PCD and 12.5 ± 1.4 for 300PCD. The λ2 also decreases to 5.8 ± 0.7 for 200PCD and 3.2 ± 0.5 for 300PCD. The dendrite fragmentation through the solidification produces a refined structure composed of equiaxed and cellular grains.

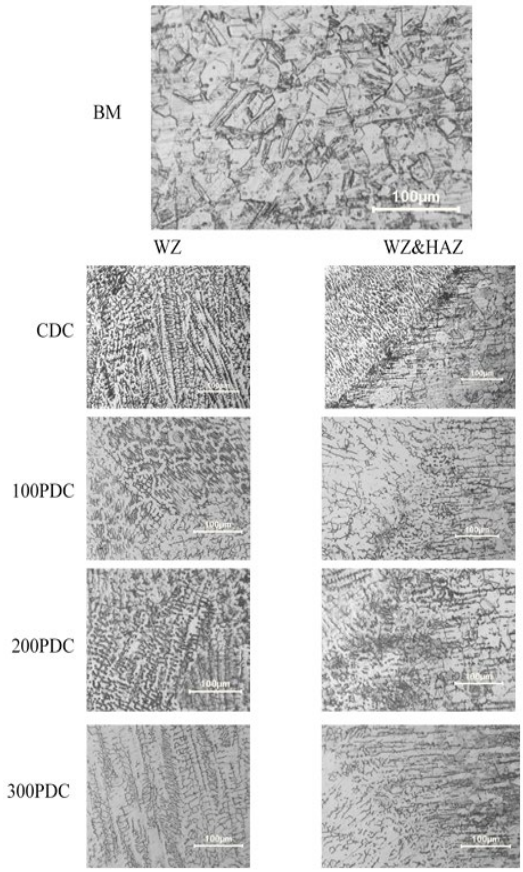


Figure 7. Microstructure for BM, WZ, and HAZ for CDC, 100PDC, 200PDC, and 300PDC
Note: Base metal (BM), weld zone (WZ), heat-affected zone (HAZ), continuous direct current (CDC), pulsed direct current (PDC).

Table 4. Grain size and dendrite spacing

Welding Condition	λ1 (μm)	λ2 (μm)	Heat-Affected Zone (HAZ) (μm)	Solidification and Grain Morphology Features
CDC	28.4 ± 3.1	9.6 ± 1.2	42.5 ± 4.8	Highly oriented directional columnar dendrites. Severe thermal grain coarsening in the HAZ.
100PDC	24.2 ± 2.8	8.1 ± 1.0	36.8 ± 3.9	Columnar dendritic growth fronts with minor branch narrowing; prominent grain growth persists in the HAZ.
200PDC	18.6 ± 1.9	5.8 ± 0.7	29.4 ± 3.2	Fragmented columnar dendritic cores transitioning to cellular structures; suppressed HAZ grain growth.
300PDC	12.5 ± 1.4	3.2 ± 0.5	22.1 ± 2.4	Highly fragmented fine cellular dendritic network with highly restricted HAZ grain boundaries.

Note: Continuous direct current (CDC), pulsed direct current (PDC).

The Higher pulse frequency effectively agitates the molten pool through thermal cycling and dynamic fluid forces. Solidification forces fragment the delicate tips of the growing dendrites. Detached fragments act as new nucleation sites in

the molten weld metal. Nucleation creates a dense network of grains instead of large columnar structures. Grain refinement stabilizes the microhardness values and increases the tensile strength. The summary of grain sizes across the welding joints is listed in Table 4.

3.3 Microhardness profile and structural homogeneity

The microhardness profile of the CDC joint appears in Figure 8(a). Hardness at the weld center decreases sharply to approximately 190 HV. It is lower than the BM (approximately 195–200 HV). There are drastic spikes in the HAZ (up to 220 HV). This uneven distribution creates severe stress concentration points that increase joint susceptibility to localized yielding and premature failure. Low and medium frequency pulsing modes 100PDC and 200PDC exhibit a shifting hardness profile. Hardness in the weld center reaches a peaks near 210 HV in Figures 8(b) and 8(c). Soft zones with hardness values dropping to 180 HV remain present in the HAZ. The 300PDC mode shown in Figure 8(d) displays the most uniform hardness distribution at 203.6 HV reflecting a uniform metallurgical structure. CDC mode resulted in a softened WZ (191.5 HV) and high HAZ hardness at 223 HV which introduced stress concentration sites. This hardness stability directly explains the higher failure strain in the 300PDC samples because deformation occurs uniformly without localized necking at the soft zones.

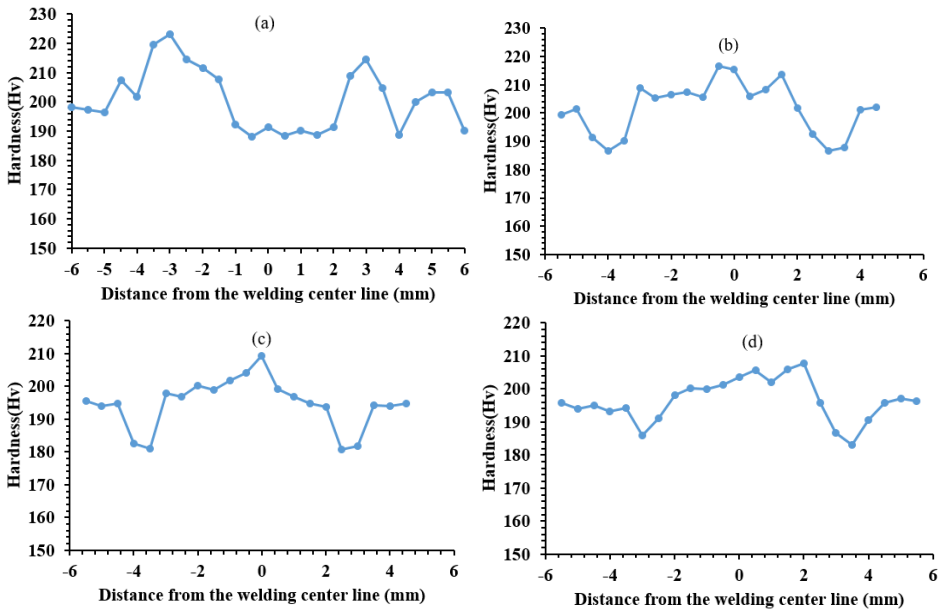


Figure 8. The microhardness profiles: (a) CDC, (b) 100PDC, (c) 200PDC, and (d) 300PDC
Note: Continuous direct current (CDC), pulsed direct current (PDC).

3.4 Corrosion resistance and phase integrity

The potentiodynamic polarization curves in Figure 9 show the relationship between the microstructural refinement and the alloy chemical stability. The shift in corrosion potential to a more noble value and the significant reduction in corrosion current density for the PDC samples relative to the CDC weldment indicate a superior resistance to oxidative attack.

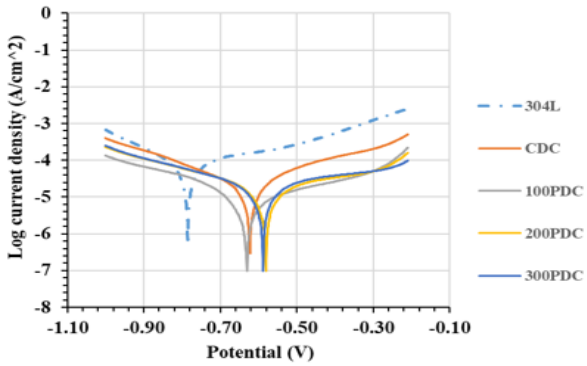


Figure 9. The potentiodynamic polarization curves

All welded joints shift to more noble potentials compared to the 304L BM. The 300PDC condition exhibits the lowest corrosion current density corresponding directly to the low corrosion rate as shown in Figure 10. This improvement in corrosion resistance is attributed to the homogeneous distribution of alloying elements induced through pulsing. The slower cooling rate in CDC welding leads to coarser dendritic structures. It is broadly reported in the literature that this induces localized chromium depletion at the grain boundaries. Rapid thermal cycling in pulsed current documented by Balasubramanian et al. [21] produce a finer and more discrete distribution of secondary phases. This prevents the formation of continuous corrosive zones and consequently stabilizing the passive chromium oxide film across the weldment.

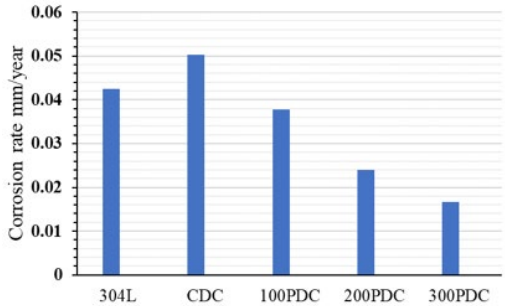


Figure 10. The corrosion rate for 304L and all welding joints

The improved chemical stability of the joint is a direct consequence of the thermal management provided by pulsing. Established metallurgical principles for 304L indicates that high pulse frequency maintains the optimal δ-ferrite phase balance required to prevent pitting. The 300PDC mode decreases the residence time in the critical temperature range for chromium carbide precipitation through HAZ constriction and refining the grains. The refined homogeneous microstructure observed at 300 Hz ensures a continuous passive layer rich in chromium that is vital to maintain the excellent corrosion resistance demonstrated by the BM.

A comparison of the mechanical and electrochemical properties obtained across all welding conditions is summarized in Table 5.

Table 5. Summary of mechanical and corrosion properties across experimental conditions

Welding Condition	Sample Size (n)	UTS (MPa)	Failure Strain/Elongation	Microhardness (HV)	Corrosion Potential (E_{corr}, V vs. Ag/AgCl)	Corrosion Current Density (I_{corr}, μA/cm^2)	Corrosion Rate (mm/year)
BM	3	735 ± 48	0.49 ± 0.055	195.0–200.0	-0.79	3.73	0.0425
CDC	3	489 ± 49	0.31 ± 0.055	191.5 (WZ)/223.0 (HAZ peak)	-0.62	4.34	0.0503
100PDC	3	529 ± 49	0.36 ± 0.055	210.0 (WZ peak)/186.0 (HAZ min)	-0.63	3.27	0.0378
200PDC	3	682 ± 47	0.58 ± 0.055	209.0 (WZ peak)/180.0 (HAZ min)	-0.58	2.11	0.0240
300PDC	3	686 ± 49	0.58 ± 0.055	203.6 ± 6.2 (Uniform WZ)	-0.59	1.46	0.0167

Note: Ultimate tensile strength (UTS), base metal (BM), continuous direct current (CDC), pulsed direct current (PDC).

4. CONCLUSIONS

Studying the effect of changing the welding current mode from CDC to PDC in joining 2 mm AISI 304L stainless steel yields the following conclusions:

1. High-frequency pulse modes (200 Hz and 300 Hz) demonstrate superior performance for thin-gauge 304L welding. 300PDC achieved an UTS of 686 MPa (93% joint efficiency) compared to only 530 MPa for continuous and low-frequency (100 Hz) modes. 300 Hz pulsing improves a failure strain (0.58) that markedly exceeds the base metal's elongation (0.48).
2. The 300 Hz pulse frequency provides the maximum refinement by transforming the solidification morphology from coarse directional columnar dendrites to a fine dendritic network. This structural refinement, as well as the narrowed HAZ, improves the mechanical performance observed in the high-frequency samples.
3. PDC reduces the hardness variation across the weldment. CDC causes softening in the WZ (191.5 HV) and erratic HAZ spikes (223 HV). The 300 Hz mode stabilizes a consistent average of 203.6 HV in the WZ as a result of the uniform plastic deformation during loading.
4. The use of a 300 Hz pulse improves chemical stability and reduces the corrosion rate to below that of the BM. This is attributed to the potential preservation of an optimal δ-ferrite phase balance and a reduced risk of sensitization typically related to the high heat input of the CDC condition. The refined homogeneous microstructure is expected to promote a continuous chromium-rich passive layer across the joint.
5. A high mechanical performance and homogeneous microstructure are required for 2 mm 304L stainless steel applications. The optimal processing parameter of 300PDC joint is carried out by using ER308L filler metal and an EWTH-1 electrode.

REFERENCES

[1] Mondal, A., Pradhan, S., Mitra, S., Dash, K., Samanta, N., Paul, T. (2021). Effect of process parameters on pulse TIG welding for stainless steel 304. International Journal of Engineering Research & Technology (IJERT), 9(11): 245-248. https://doi.org/10.17577/IJERTCONV9IS11058

[2] Afify, R., Abdel-Aleem, H.A., Gamil, M. (2024). Investigating TIG arc weldments for austenitic stainless steel 304 and 304L: A mechanical and metallurgical analysis. Engineering Research Journal (Shoubra), 53(1): 181-188. https://doi.org/10.21608/erjsh.2023.228930.1205

[3] Zheng, X., Zhao, K., Jing, J., Li, H. (2025). Microstructure, mechanical properties and corrosion resistance of tungsten inert gas welded joints of selective laser melting 304L stainless steel. Materials Today Communications, 46: 112533. https://doi.org/10.1016/j.mtcomm.2025.112533

[4] Widyianto, A., Baskoro, A.S., Kiswanto, G. (2022). Investigation on weld characteristic, welding position, microstructure, and mechanical properties in orbital pulse current gas tungsten arc welding of AISI 304L stainless steel pipe. International Journal of Technology, 13(3): 473-483. https://doi.org/10.14716/ijtech.v13i3.3134

[5] Kumar, P., Sinha, A.N., Hirwani, C.K., Murugan, M., Saravanan, A., Singh, A.K. (2021). Effect of welding current in TIG welding 304L steel on temperature distribution, microstructure and mechanical properties. Journal of the Brazilian Society of Mechanical Sciences and Engineering, 43(7): 369. https://doi.org/10.1007/s40430-021-03082-6

[6] Ugla, A.A. (2018). Enhancement of weld quality of AISI 304L austenitic stainless steel using a direct current pulsed TIG arc. IOP Conference Series: Materials Science and Engineering, 433(1): 012075.

https://doi.org/10.1088/1757-899X/433/1/012075
[7] Sohail, A., Aziz, A., Imran, M., M, O.J., Ahmed, S. (2017). Effect of TIG welding parameters on the properties of 304L automated girth welded pipes using orbital welding machine. Research Reviews: Journal of Material Science, 5(4): 136-143. https://doi.org/10.4172/2321-6212.1000201
[8] Shah, P., Agrawal, C. (2019). A review on twin Tungsten Inert Gas welding process accompanied by hot wire pulsed power source. Journal of Welding and Joining, 37(2): 41-51. https://doi.org/10.5781/JWJ.2019.37.2.7
[9] Lothongkum, G., Chaumbai, P., Bhandhubanyong, P. (1999). TIG pulse welding of 304L austenitic stainless steel in flat, vertical and overhead positions. Journal of Materials Processing Technology, 89: 410-414. https://doi.org/10.1016/S0924-0136(99)00046-1
[10] Saha, S., Das, S., Mondal, S. (2025). Experimental investigation on autogenous TIG and A-TIG welding for enhanced penetration in austenitic SS304H flats. Indian Welding Journal, 58(1): 75-82. https://doi.org/10.22486/iwj.v58i1.48809
[11] Sahoo, A., Tripathy, S. (2021). Improvement in depth of weld penetration during TIG, activated-TIG, and pulsed TIG welding: A review. International Journal of Manufacturing, Materials, and Mechanical Engineering (IJMMME), 11(2): 68-86. https://doi.org/10.4018/IJMMME.2021040105
[12] Ramkumar, K.D., Singh, S., George, J.C., et al. (2017). Effect of pulse density and the number of shots on hardness and tensile strength of laser shock peened, activated flux TIG welds of AISI 347. Journal of Manufacturing Processes, 28(Part 1): 295-308. https://doi.org/10.1016/j.jmapro.2017.06.017
[13] Tong, Z., Zhentai, Z., Rui, Z. (2013). A dynamic welding heat source model in pulsed current gas tungsten arc welding. Journal of Materials Processing Technology, 213(12): 2329-2338. https://doi.org/10.1016/j.jmatprotec.2013.07.007
[14] Wang, Z., Jiang, D., Wu, J., Xu, M. (2020). A review on high-frequency pulsed arc welding. Journal of Manufacturing Processes, 60: 503-519. https://doi.org/10.1016/j.jmapro.2020.10.054
[15] Sabzi, M., Anijdan, S.H.M., Chalandar, A.R.B., Park, N., Jafarian, H.R., Eivani, A.R. (2022). An experimental investigation on the effect of gas tungsten arc welding current modes upon the microstructure, mechanical, and fractography properties of welded joints of two grades of AISI 316L and AISI310S alloy metal sheets. Materials Science and Engineering: A, 840: 142877. https://doi.org/10.1016/j.msea.2022.142877
[16] Kondapalli, S., Chalamalasetti, S.R., Damera, N.R. (2013). Application of grey relational analysis for optimizing weld pool geometry parameters of pulsed current micro plasma arc welded AISI 304L stainless steel sheets. International Journal of Advanced Design and Manufacturing Technology, 6(1): 79. https://www.proquest.com/openview/02085a27c00788f84b87525c725d39ec/1?pq-origsite=gscholar&cbl=696402.
[17] ASTM E8. (2001). Standard Test Methods for Tension Testing of Metallic Materials. ASTM International, West Conshohocken, PA. https://doi.org/10.1520/E0008-01
[18] AWS, B4.0:2007. (2007). Standard Methods for Mechanical Testing of Welds. American Welding Society.
[19] ASTM E407-07. (2011). Standard Practice for Microetching Metals and Alloys. ASTM International, West Conshohocken, PA. https://doi.org/10.1520/E0407-07
[20] ASTM International. (2015). Standard practice for calculation of corrosion rates and related information from electrochemical measurements (ASTM G102-89). West Conshohocken, PA. https://doi.org/10.1520/G0102-89R15
[21] Balasubramanian, M., Jayabalan, V., Balasubramanian, V. (2010). Effect of process parameters of pulsed current tungsten inert gas welding on weld pool geometry of titanium welds. Acta Metallurgica Sinica (English Letters), 23(4): 312-320. https://doi.org/10.11890/1006-7191-104-312